NEAR- AND MID-INFRARED LABORATORY SPECTRA OF PAH CATIONS IN SOLID H₂O

M. P. BERNSTEIN, S. A. SANDFORD, A. L. MATTIODA, AND L. J. ALLAMANDOLA

NASA-Ames Research Center, Mail Stop 245-6, Moffett Field, CA 94035-1000; mbernstein@mail.arc.nasa.gov

ABSTRACT

Polycyclic aromatic hydrocarbons (PAHs) have been observed in absorption along lines of sight toward embedded protostars. In such cold space environments PAHs should condense into H_2O-rich ice mantles at low temperature and be exposed to ionizing radiation. In this paper we present the first infrared spectra of PAH cations in solid H_2O generated under conditions that resemble dense molecular clouds. After exposing PAHs in solid H_2O at 15 K to low doses of UV radiation, we have observed both the vibrational absorptions of PAH cations in the mid-IR and electronic transitions in the near-IR. The PAHs observed as ions in solid H_2O were naphthalene, anthracene, phenanthrene, benzo[k]fluoranthene, and benzo[ghi]perylene. Peak positions, strengths, and temperature dependence are reported for the detected ion bands, and their astrophysical significance is discussed. These laboratory measurements suggest that absorption bands of PAH cations in H_2O ice may be observable by astronomers in the near- and mid-infrared.

Subject headings: astrobiology — astrochemistry — infrared: ISM — infrared: solar system —
ISM: lines and bands — ISM: molecules — methods: laboratory

1. INTRODUCTION

Polycyclic aromatic hydrocarbons (PAHs) and related aromatic materials are proposed to be present in virtually all phases of the interstellar medium (ISM; Allamandola et al. 1999; Cox & Kessler 1999), including lines of sight toward protostellar objects. Infrared (IR) absorptions attributed to PAHs have been observed in spectra of objects embedded in dense clouds including features near 3030 cm^{-1} (3.3 μm; Smith et al. 1989; Sellgren et al. 1995; Brooke et al. 1999), 1600 cm^{-1} (6.2 μm; Chiar et al. 2000), and 890 cm^{-1} (11.2 μm; Bregman et al. 2000). H_2O is by far the most abundant solid component present along these lines of sight, suggesting the possibility that some of the PAHs responsible for these absorption bands may be condensed into H_2O-rich ices. We have previously presented laboratory IR spectra of neutral PAHs in H_2O (Sandford et al. 2004; Bernstein et al. 2005) for comparison to the interstellar absorption features, but to our knowledge no IR spectra of PAH cations in H_2O ices exist in the literature.

In our first paper on the ultraviolet (UV) photochemistry of PAHs in H_2O (Bernstein et al. 1999), we hypothesized, and then others calculated (Ricca & Bauschlicher 2000), that PAH cations are possible intermediates in the reaction(s) that formed oxidized PAHs. However, even if this were true, it does not necessarily follow that PAH ion intermediates would be abundant enough in the ices to be observed. However, the electronic transitions of PAH cations in solid H_2O were observed by Gudipati (2004) and Gudipati & Allamandola (2006), suggesting that they can be present at abundances high enough that absorptions of PAH cations in solid H_2O might be observable in the mid-IR. This prompted us to generate PAH cations in solid H_2O, and identify their IR absorptions by comparison with previously measured spectra of PAH cations isolated in argon matrices (e.g., Hudgins & Allamandola 1995a, 1995b; Hudgins et al. 2000).

It is to be hoped that this report of IR absorptions of PAH cations in H_2O ice will facilitate the detection of PAH cations in dense molecular clouds where neutral PAHs have already been reported in absorption (Smith et al. 1989; Sellgren et al. 1995; Brooke et al. 1999; Chiar et al. 2000; Bregman et al. 2000). In addition, detections of aromatics on icy Saturnian satellites (Clark et al. 2005; Cruikshank et al. 2005, 2007) via the Visual IR Mapping Spectrometer (VIMS) aboard the *Cassini* spacecraft

suggest that PAH cations in H_2O could also be present in our own solar system.

Finally, we have shown that low-temperature PAH photochemistry produces oxidized aromatic compounds (Bernstein et al. 1999, 2003) much like those in meteorites (Cronin & Chang 1993; Cody & Alexander 2005) and interplanetary dust particles (IDPs; Flynn et al. 2004). Studies of the organic molecules in primitive meteorites and IDPs show these objects contain deuterium enrichments that are best explained by an interstellar dense cloud chemical heritage (Sandford et al. 2000; Sandford 2002), consistent with reactions involving PAH cations in H_2O ice at low temperature. Thus, this work also pertains to those branches of astrobiology and meteoritics that examine the organic matter delivered to the Earth by meteorites and IDPs, a majority of which are aromatic.

The experimental techniques used for this work are summarized in § 2, and the data obtained from the various PAH cations in H_2O are shown in § 3. Some interpretations of the laboratory results and astrophysical implications are presented in § 4.

2. EXPERIMENTAL TECHNIQUES

2.1. *Sample Preparation*

The H_2O-PAH samples studied in this paper were vapor deposited as submicron-thick films on a CsI window. The window was held at ∼15 K and was suspended in an evacuated sample chamber at a pressure of ∼10^{-8} torr. Detailed descriptions of the deposition process and apparatus can be found elsewhere (Hudgins & Allamandola 1995a; Mattioda et al. 2005).[1]

All the PAHs examined in this study are solids at room temperature and, except for naphthalene ($C_{10}H_8$), all have a fairly low vapor pressure. As a result, only the H_2O-naphthalene samples were deposited from a bulb premixed in the gas phase at room temperature before deposition, as was done in our previous study on the IR spectra of neutral naphthalene in H_2O (Sandford et al. 2004). For all the other compounds, H_2O and the PAH under study were codeposited onto the CsI substrate through separate inlets. In both cases the H_2O was deposited from a gas bulb containing H_2O
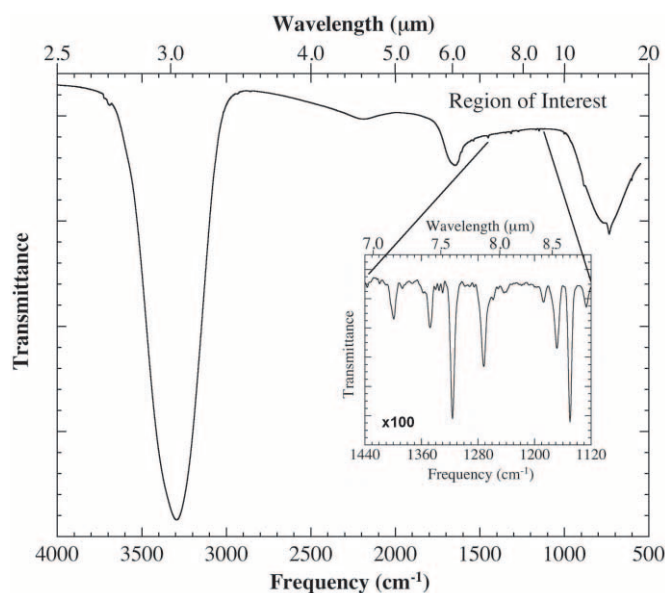
---

[1] See also http://www.astrochemistry.org.

Fig. 1.—The 4000–500 cm^{-1} (2.5–20 μm) IR transmission spectrum of a solid H$_2$O-anthracene (C$_{14}$H$_{10}$) mixture (H$_2$O/C$_{14}$H$_{10}$ $\sim$ 70) at 15 K. The large broad absorptions in the spectrum centered near 3300, 1650, and 750 cm^{-1} (3.0, 6.1, and 13.3 μm) are caused by the amorphous solid H$_2$O. At this concentration, H$_2$O absorptions dominate the spectrum, and many of the anthracene features are obscured. The peaks of anthracene are most obvious in the 1440–1120 cm^{-1} (6.94–8.93 μm) region of the spectrum that appears inset, expanded, and magnified 100 times.

Fig. 2.—The 1440–1120 cm^{-1} (6.94–8.93 μm) IR transmission spectra of the PAH anthracene (C$_{14}$H$_{10}$) and its cation. The top two spectra are of anthracene isolated in solid argon at 15 K (line "A") before and (line "B") after exposure to UV photolysis. The bottom two spectra are from anthracene frozen in solid H$_2$O at 15 K (line "C") before and (line "D") after exposure to UV photolysis. The peaks of the anthracene cation in argon previously assigned by Hudgins & Allamandola (1995b) are marked with dashed lines connecting them to the presumed peaks of the anthracene cation in solid H$_2$O. These spectra are displayed on the same scale, but offset for clarity. The peak marked with an "x" is a photoproduct of H$_2$O.

vapor prepared from a liquid sample on a glass manifold with a background pressure of $\sim$1 $\times$ 10^{-5} mbar. Since the pressures in the H$_2$O sample bulbs were 10–20 mbar, contaminant levels associated with the H$_2$O were negligible. The flow rate of H$_2$O onto the cold window was controlled by a microflow meter and by the pressure of H$_2$O in the bulb.

The PAHs were sublimed onto the substrate from a Pyrex tube wrapped in resistive heating wire (see Hudgins & Allamandola 1995a). The temperature to which the tube was heated depended on the sublimation point of the PAH in question and the approximate H$_2$O/PAH ratio desired. The temperatures used for deposition of the different PAHs were: anthracene (60°C), phenanthrene (130°C), benzo[k]fluoranthene (130°C), and benzo[ghi]perylene (150°C).

The PAH sample tube takes minutes to come up to temperature, and thus, it takes minutes for the PAHs to reach a steady rate of sublimation. To prepare samples with a uniform PAH concentration, we bring the PAH tube up to temperature with the substrate in a position shielded from the sample inlets. In all cases the samples were not permitted to deposit onto the CsI substrate until after the temperature of the PAH sample tube and the H$_2$O flow rate had stabilized. Similarly, the sample deposition was halted by rotating the sample to the shielded position as well as shutting off the flow of sample.

The H$_2$O-PAH sample gases were typically codeposited onto the 15 K CsI window at a rate that produced an $\sim$0.1 μm thick ice layer after a few minutes of deposition based on the observed strengths of the H$_2$O absorption features in the sample spectra (see § 2.2). This deposition technique produces an ice composed of an intimate mixture of the PAH molecules in H$_2$O. We know that pure H$_2$O deposited under these conditions is in its high-density amorphous form (Jenniskens & Blake 1994; Jenniskens et al. 1995). Our IR spectra of neutral PAHs in H$_2$O ices are consistent with the H$_2$O being amorphous (Sandford et al. 2004; Bernstein et al. 2005), the dominant form of H$_2$O ice present in
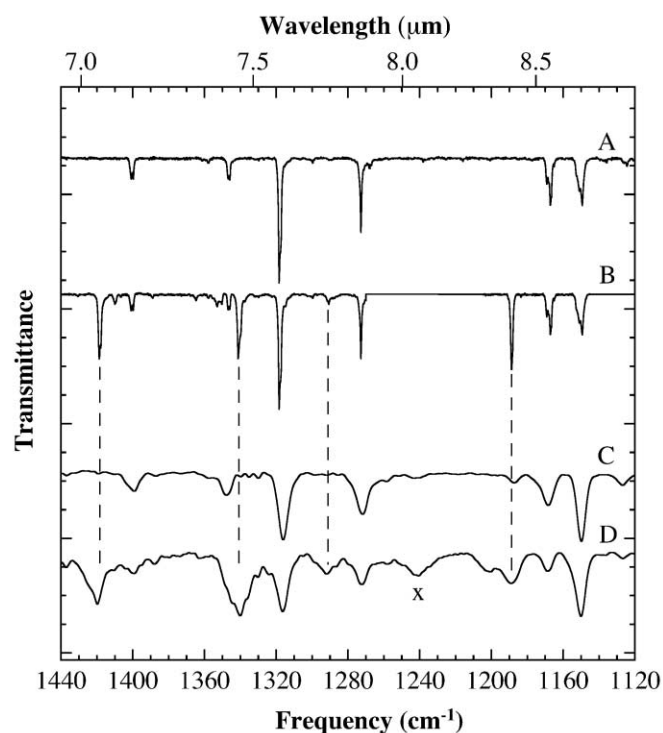
interstellar molecular clouds (Allamandola & Sandford 1988; Jenniskens & Blake 1994; Jenniskens et al. 1995).

After deposition onto the CsI window, IR spectra of the samples were measured at a resolution of 1 cm^{-1} with a Biorad FTS 3000 spectrometer with LN$_2$-cooled mercury cadmium telluride (MCT) detector and salt beamsplitter for the mid-IR and an ambient temperature deuterated triglycine sulfate (DTGS) detector and quartz beamsplitter for the near IR. Analyses of the areas of the resulting IR absorption bands of both the H$_2$O and PAHs verified that our sample ice layers had thicknesses of a few tenths of a micron and had H$_2$O/PAH ratios falling between 30 and 100 (see § 2.2). In some cases, additional spectra were subsequently measured after the samples had been warmed to temperatures of 50 and 100 K. Samples were warmed at a rate of $\sim$2 K minute^{-1} between the temperature steps and were allowed to equilibrate for more than 5 minutes at each temperature before spectra were taken.

The H$_2$O used in these experiments was purified via a Millipore Milli-Q water system to 18.2 MΩ and freeze/pump/thawed three times in vacuum to remove dissolved gases prior to use. The PAHs (purchased from the Aldrich Chemical Company unless otherwise noted) were used without any further purification, and were reported to have the following purities: naphthalene (99%), anthracene (99%), phenanthrene (99.5%+), benzo[k]fluoranthene (Janssen Chimica; 99%+), and benzo[ghi]perylene (98%).

UV photolysis was performed using a microwave-excited hydrogen flow lamp with a "McCarrol" cavity from Opthos, as described in detail elsewhere (Warneck 1962). This lamp produces $\sim$10^{15} photons cm^{-2} s^{-1} evenly divided between Lyα photons at 1216 Å and a several hundred nm wide broad emission band

TABLE 1
Mid-IR Cation Absorptions of PAHs in Argon vs. H$_2$O

| PAH | PAH Cation in Argon[a] | | PAH Cation in H$_2$O | |
	Position (cm^{-1})	Relative Area	Position (cm^{-1})	Relative Area
Naphthalene	1215, 1218	N/A (see text)	1217[b]	N/A (see text)
Anthracene	1188.6	0.7	1189	0.76
	1290.4	0.058	1291	0.29
	1341.0 + 1352.6	1.0 + 0.31	1340[b]	1.0[b]
	1409.5	0.11	sh 1411	
	1418.4	0.86	1419	0.6
Phenanthrene	1136.3 + 1139.7	0.072 + 0.065	sh 1134[b,c] 1140[b,c]	1.4[b,c]
	1258.7 + 1264.7 + 1267.0	0.055 + 0.016 + 0.16	1263	0.51
	1282.5, 1277.5	1.0	1285	1.0
	1299.0	0.11		
	1565.0	0.54	1566	0.71
Benzo[k]fluoranthene	1292.3 + 1306.0	0.34 + 0.026	1290[b]	0.62[b]
	1320.7	1.0	1320	1.0
	1335.4 + 1337.7	0.0048 + 0.086	1339[b]	0.16[b]
	1380.2, 1383.7	0.11	1385	0.13
Benzo[ghi]perylene................	1140.2	0.39	1145[b,c]	0.37[b,c]
	1216.7 + 1223.4	0.033 + 0.3	1223	?[c]
	1311.9	0.14	?[b]	
	1324.4	0.74	1325	0.12
	1331.9	0.17	?	
	1350.2	0.15	1353	0.29
	1369.0	0.62	?	
	1388.3 + 1401.3 + 1408.8	0.032 + 0.83 + 0.046	1402.9	0.88
	1429.4	0.096	1423	0.14
	1538.6	0.018	1531	0.18
	1550.1	0.22	1551	0.2
	1578.2	1.0	1579	1.0

[a] The values for PAH cations isolated in solid argon were taken from our Web page (at http://www.astrochem.org/databases.htm) and appeared in previously published papers (Hudgins & Allamandola 1995a,1995b; Hudgins et al. 2000).

[b] Overlap with an absorption from neutral PAH makes cation peak positions, widths, and areas difficult to calculate.

[c] Known H$_2$O photolysis products produce peaks near 1139 and 1235 cm^{-1}, which make areas and positions of peaks near these locations uncertain.

centered at ∼1600 Å. Typical samples were photolyzed for only a few minutes, corresponding to a dose of ∼3 × 10^{17} photons cm^{-2}, equivalent to roughly 10^7 yr in a dense cloud assuming the most conservative UV flux based solely on the cosmic-ray–induced UV photons at a rate of 1 × 10^3 cm^{-2} s^{-1} (Prasad & Tarafdar 1983).

2.2. H$_2$O/PAH Sample Ratios

With H$_2$O-naphthalene mixtures it was possible to carefully control the H$_2$O/C$_{10}$H$_8$ ratios by premixing samples in the gas phase. The other PAHs considered in this work have vapor pressures that are too low for gas-phase mixing, making it difficult to precisely control the ultimate H$_2$O/PAH ratio of the ice samples. We estimated the H$_2$O/PAH ratio of each sample after deposition by integrating H$_2$O and PAH peaks and ratioing the numbers of molecules calculated from the band strengths. We determined the H$_2$O column density by measuring the areas of the O—H stretching mode (3300 cm^{-1}; 3.0 μm) and H—O—H bending mode (1660 cm^{-1}; 6.0 μm) bands of H$_2$O ice and assuming inherent strengths of 1.7 × 10^{-16} and 1.0 × 10^{-17} cm molecule^{-1}, respectively (Hudgins et al. 1993). The column density of the given PAH in a sample was estimated by measuring the areas of multiple bands of the neutral PAH and using their calculated gas-phase band strengths (Langhoff 1996, Hudgins & Sandford 1998a, 1998b, 1998c). This method is expected to provide a good estimate of PAH column density, since our previous work on the

H$_2$O-naphthalene and other H$_2$O-PAH systems has demonstrated that the presence of the H$_2$O produces modest changes in the relative band strengths of most PAH bands (Sandford et al. 2004; Bernstein et al. 2005). For all the PAHs but naphthalene, this method gave concentrations of PAHs relative to H$_2$O in the range of 1%–3%, so the PAHs in all our samples were in an H$_2$O-dominated environment (see, for example, Fig. 1). For naphthalene we were able to control the concentration by premixing the H$_2$O and naphthalene in the gas phase. This allowed us to examine the effect of concentration on ionization efficiency for this PAH. We performed photolysis on samples with naphthalene concentrations of ∼1% and 10% relative to H$_2$O (see, for example, Fig. 10).

The proportions of PAH ionized by photolysis were estimated by measuring the areas of the new ion bands and using literature values for the absorption strengths of the PAH cations studied in argon matrices (Hudgins & Allamandola 1995a, 1995b). PAH ion abundances determined in this manner provided ion yields in general agreement with complementary estimates based on measuring the simultaneous loss of the original PAH neutrals. The conversion of neutral PAHs to PAH ions is the dominant radiation process at low temperature and low concentrations (Gudipati & Allamandola 2006), as opposed to oxidation or reduction reactions, for example (Bernstein et al. 1999). Our estimates of the fraction of the neutral PAH ionized on exposure of our H$_2$O/PAH mixtures to UV photolysis is consistently higher than that
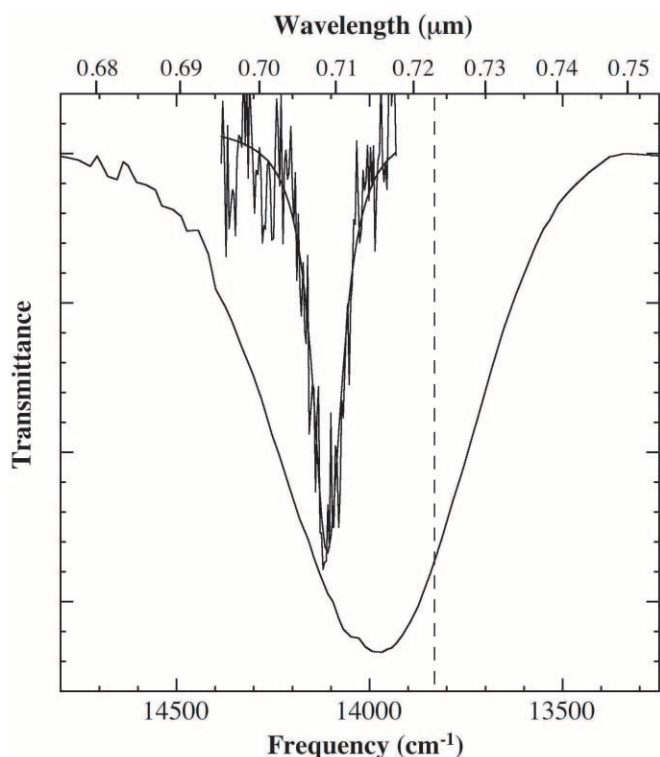
FIG. 3.—The 14,800–13,250 cm^{-1} (0.676–0.755 μm) near-IR transmission spectrum of anthracene in H$_2$O after exposure to UV photolysis at 15 K (*bottom*) compared to that of the anthracene cation (C$_{14}$H$_{10}^+$) in the gas phase (*top*) from Sukhorukov et al. (2004). A dashed vertical line at 13,832 cm^{-1} (0.72296 μm) indicates the position of the anthracene cation isolated in an argon matrix (from Table II of Hudgins & Allamandola 1995b). We assign the broad band centered near 14,000 cm^{-1} (0.714 μm) to the anthracene cation in solid H$_2$O.

observed for PAHs isolated in argon (e.g., Hudgins & Allamandola 1995a, 1995b), but less than that observed by Gudipati & Allamandola (2006) (see § 4.1).

3. RESULTS

The mid-IR spectra of H$_2$O-PAH mixes with astrophysically relevant concentrations of PAHs are dominated by the strong vibrational-mode bands of H$_2$O, as is exemplified in the 4000–500 cm^{-1} (2.5–20 μm) mid-IR spectrum of an H$_2$O/anthracene ≈ 70 sample shown in Figure 1. The prominent absorptions in the spectrum in Figure 1 near 3300, 1650, and 750 cm^{-1} (3.0, 6.1, and 13.3 μm) are those of the O—H stretch, H—O—H bend, and librational modes of the H$_2$O, respectively.

The presence of ∼1% PAH (anthracene in the case of Fig. 1) produces additional, weaker, sharper peaks superimposed on the broad H$_2$O bands. This is typical for the IR spectra of neutral PAHs at these concentrations in H$_2$O (Sandford et al. 2004; Bernstein et al. 2005). The peaks of neutral anthracene seen in Figure 1 are least obscured in the region between the 1650 and 750 cm^{-1} H$_2$O features, and the 1440–1120 cm^{-1} (6.94–8.93 μm) region appears inset, expanded, baseline-corrected, and magnified 100 times in transmittance. It is in spectra of this sort that new cation bands must be identified after such ices are UV photolyzed.

3.1. *IR Spectra of PAH Cations in* H$_2$O

3.1.1. *Anthracene* (C$_{14}$H$_{10}$)

In previous work by Szczepanski et al. (1993) and Hudgins & Allamandola (1995b) it had been shown that when anthracene isolated in argon was exposed to UV photolysis, some of the neutral starting anthracene was converted to cations. The positions and strengths of the absorptions of the anthracene cation in argon were reported in their papers. We exposed the H$_2$O/anthracene ≈ 70 mixture (shown above in Fig. 1) to exactly the same lamp and dose of UV photolysis that Hudgins & Allamandola (1995b) used to produce the anthracene cation in argon and obtained completely analogous results.

In Figure 2 we return to the 1440–1120 cm^{-1} (6.94–8.93 μm) region of the IR spectrum seen inset in Figure 1, but now focusing on changes that occur with UV photolysis. The top two traces are spectra of anthracene isolated in solid argon at 15 K before (Fig. 2, line "A") and after (line "B") exposure to UV photolysis, and the bottom two are spectra of the above H$_2$O/anthracene ≈ 70 mixture at 15 K before (line "C") and after (line "D") exposure to UV photolysis. The peaks of the anthracene cation in argon previously assigned by Hudgins & Allamandola (1995b) are marked with dashed lines connecting them to the new peaks produced by UV photolysis of the H$_2$O-anthracene sample.

There is a remarkable correspondence, both in position and relative intensity, between the peaks of the anthracene cation in argon and the new bands in the spectrum of H$_2$O/anthracene ≈ 70 after exposure to UV photolysis. An exception in this and some subsequent experiments is a new peak near ∼8.06 μm (1240 cm^{-1}), which we routinely see in pure H$_2$O photolysis control experiments, suggesting this is simply an H$_2$O photolysis product. The relative areas of the peaks of neutral anthracene diminish by ∼30% on average after photolysis, suggesting that approximately one-third of the starting anthracene has been converted to another species, presumably the cation. The positions and relative intensities for these and all subsequent mid-IR cation peaks can be found in Table 1.

In addition to the new *mid*-IR features (seen in Fig. 2) exposure of the H$_2$O/anthracene ≈ 70 mixture to UV photolysis also produces a strong new absorption in the near-IR that is consistent with the anthracene cation. Figure 3 shows the 14,800–13,250 cm^{-1} (0.676–0.755 μm) near-IR spectrum of the same H$_2$O/anthracene ≈ 70 mixture after exposure to UV photolysis at 15 K (*bottom*) compared to that of the anthracene cation (C$_{14}$H$_{10}^+$) in the gas phase (*top*) from Sukhorukov et al. (2004). A dashed vertical line at 13,832 cm^{-1} (0.72296 μm) indicates the position of the anthracene cation in argon (Hudgins & Allamandola 1995b). The broad band centered near 14,000 cm^{-1} (0.714 μm) is approximately 500–1000 times more intense than the strongest mid-IR absorption bands, consistent with its being an electronic transition of the anthracene cation (as opposed to a PAH combination/overtone mode, in which case it would be weaker, not stronger, than the mid-IR fundamentals).

3.1.2. *Benzo[k]fluoranthene* (C$_{20}$H$_{12}$)

In a manner analogous to that seen above for anthracene, new absorptions in mid- and near-IR spectra of benzo[k]fluoranthene in H$_2$O are seen after UV photolysis that are consistent with the benzo[k]fluoranthene cation in H$_2$O. Figure 4 depicts the 1400–1250 cm^{-1} (7.14–8.0 μm) IR spectra of benzo[k]fluoranthene in solid H$_2$O at 15 K (Fig. 4, line "A") before and (line "B") after exposure to UV photolysis. The four prominent new peaks (marked by an asterisk) that appear after photolysis agree with those previously assigned to the benzo[k]fluoranthene cation in argon by Hudgins et al. (2000). The new ion absorption band near 1340 cm^{-1} (7.46 μm) falls on top of one of the preexisting peaks of neutral benzo[k]fluoranthene, and blends with it because peak widths are greater in H$_2$O than in argon. However, given that the spectra are displayed on the same scale, the increased
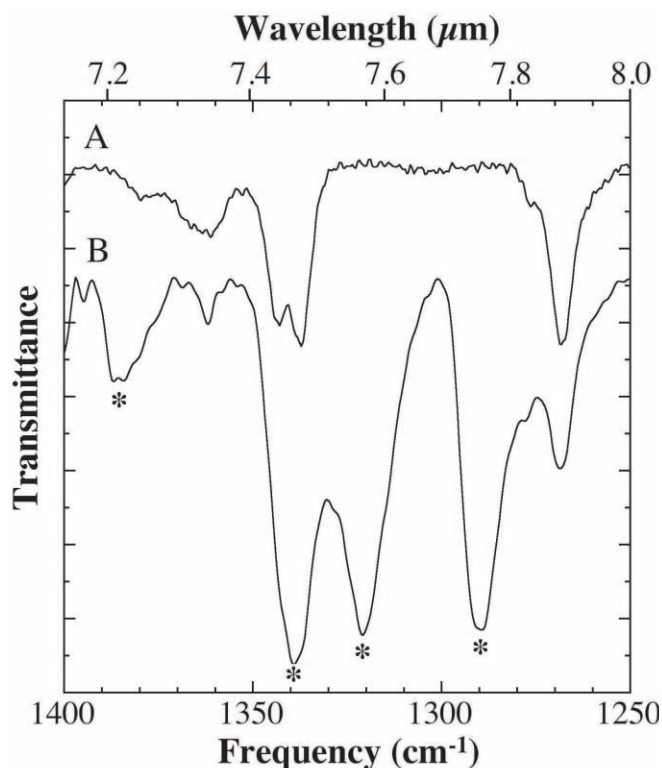
FIG. 4.—The 1400–1250 cm^{-1} (7.14–8.0 μm) IR transmission spectra of the PAH benzo[k]fluoranthene (C$_{20}$H$_{12}$) in solid H$_2$O at 15 K (line "A") before and (line "B") after exposure to UV photolysis. The four prominent new peaks marked by an asterisk (*) that appear after photolysis agree with those previously assigned to the benzo[k]fluoranthene cation in argon by Hudgins et al. (2000). Thus, we attribute these features to the benzo[k]fluoranthene cation in solid H$_2$O. The new absorption near 1340 cm^{-1} (7.46 μm) falls on top of one of the preexisting peaks of neutral benzo[k]fluoranthene. The spectra are displayed on the same scale, but offset for clarity.

FIG. 5.—The 11,000–8800 cm^{-1} (0.91–1.14 μm) near-IR transmission spectra of the PAH benzo[k]fluoranthene in solid H$_2$O after photolysis at 15 K (bottom) and after warming to 100 K (top). The broad new absorption created by photolysis centered near 9700 cm^{-1} (1.03 μm) agrees well with that at 9520 cm^{-1} (1.050 μm) assigned by Mattioda et al. (2005) to the benzo[k]fluoranthene cation in solid argon (dashed line). We note that the feature diminishes on warming, but is still present at 100 K. These spectra are displayed on the same scale, but offset for clarity.

intensity at this position makes it clear there is new absorption occurring where a new ion band would be predicted based on the argon data of Hudgins et al. (2000), see Table 1.

Based on the unobscured neutral benzo[k]fluoranthene peak at 1192 cm^{-1} (8.34 μm), which was seen to have diminished to ~60% of its original area, we estimate that ~40% of the starting PAH was converted to ion by photolysis. However, it is possible that some of the loss of starting material was a result of reaction with water to produce oxidized or hydrogenated products (Bernstein et al. 1999, 2003).

Similarly, a new strong band that appears in the near-IR spectrum of benzo[k]fluoranthene in solid H$_2$O after photolysis at 15 K (Fig. 5) is consistent with the benzo[k]fluoranthene cation. The dashed line in Figure 5 at 9520 cm^{-1} (1.05 μm) marking the location of a strong absorption of the benzo[k]fluoranthene cation in solid argon (Mattioda et al. 2005) agrees well with the broad new band near 9700 cm^{-1} (1.03 μm) seen in the spectrum of benzo[k]fluoranthene after photolysis in H$_2$O. Again, the strength of this feature suggests it is an electronic transition. Moreover, we note that this apparent cation peak is diminished after warming to 100 K at ~2 K minute^{-1}, consistent with it being an unstable species such as a cation.

3.1.3. Phenanthrene (C$_{14}$H$_{10}$)

In a manner akin to that described above, IR spectra of the PAH phenanthrene (C$_{14}$H$_{10}$) in solid H$_2$O and exposed to UV photolysis at 15 K display new peaks that are consistent with previous measurements of the phenanthrene cation in argon.
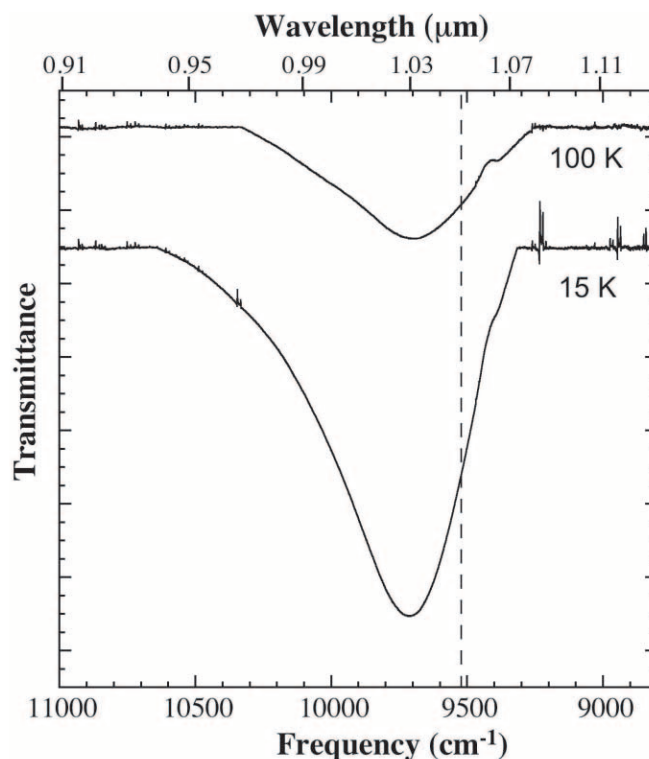
Figure 6 shows the 1350–1100 cm^{-1} (7.41–9.09 μm) IR spectra of the PAH phenanthrene in solid H$_2$O at 15 K before and after exposure to UV photolysis. Four new peaks (marked by an asterisk) agree with those previously assigned to the phenanthrene cation in argon by Hudgins & Allamandola (1995a; see also our Table 1). The new ion absorptions near 1140 cm^{-1} (8.77 μm) fall on top of a preexisting peak of neutral phenanthrene. By comparing the relative areas of the peaks of neutral phenanthrene in Figure 6 before and after photolysis, i.e., those at 1246, 1203, and 1166 cm^{-1} (8.026, 8.313, and 8.576 μm), we find that ~40% of the starting phenanthrene has been converted to another species, presumably the cation.

Figure 7 shows the position of a new near-IR band at ~11,100 cm^{-1} (0.901 μm) that is formed on UV photolysis of phenanthrene in H$_2$O. This band coincides remarkably well with that of the electronic transition of the phenanthrene cation in argon, indicated by a dashed vertical line (Hudgins & Allamandola 1995a; Mattioda et al. 2005). The absorptions in H$_2$O and argon differ by less than 10 cm^{-1} (0.001 μm). In contrast to the benzo[k]fluoranthene cation (Fig. 5), which continued to persist even after warming to 100 K, the behavior of the band in Figure 7 with warming at 2 K minute^{-1} suggests that the phenanthrene cation is not as stable under these conditions; it diminishes considerably by 50 K, and is no longer detectable by 100 K.

3.1.4. Benzo[ghi]perylene (C$_{22}$H$_{12}$)

As with the previous PAHs, IR spectra of benzo[ghi]perylene (C$_{22}$H$_{12}$) in solid H$_2$O show, on exposure to UV photolysis at 15 K, the appearance of new absorptions consistent with the
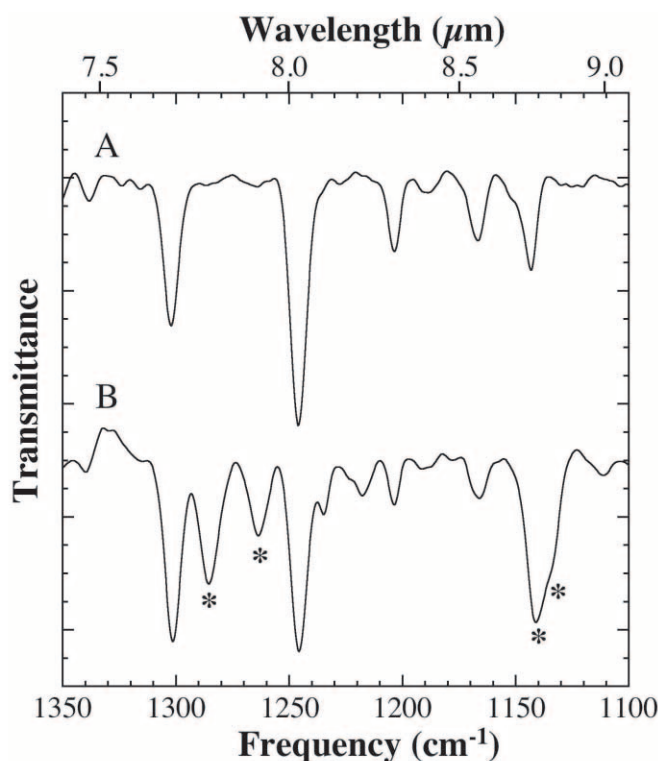
Fig. 6.—The 1350–1100 cm^{-1} (7.41–9.09 μm) IR transmission spectra of the PAH phenanthrene (C$_{14}$H$_{10}$) in solid H$_2$O at 15 K (line "A") before and (line "B") after exposure to UV photolysis. The new peaks marked by an asterisk (*) agree with those previously assigned to the phenanthrene cation in argon by Hudgins & Allamandola (1995a). We therefore attribute them to the phenanthrene cation in solid H$_2$O. The new absorptions near 1140 cm^{-1} (8.77 μm) fall on top of a preexisting peak of neutral phenanthrene. The two spectra are on the same scale, but the spectra are offset for clarity. The peaks of neutral C$_{14}$H$_{10}$ in the lower spectrum have diminished relative to those above, corresponding to conversion of 25%–30% of the original neutrals into cations.

Fig. 7.—The 12,200–10,000 cm^{-1} (0.82–1.0 μm) near-IR transmission spectra of the PAH phenanthrene in solid H$_2$O at 15 K after UV photolysis (*bottom*) and after warming to 50 and 100 K. The new broad band centered near 11,100 cm^{-1} (0.901 μm) corresponds remarkably well to that at 11,110 cm^{-1} (0.900 μm) assigned to the phenanthrene cation in argon by Hudgins & Allamandola (1995a) and Mattioda et al. (2005). We note that the feature diminishes on warming and is essentially gone by 100 K. These spectra are displayed on the same scale, but offset for clarity.

benzo[ghi]perylene cation. In Figure 8, new peaks in the 1600–1100 cm^{-1} (6.25–9.09 μm) region of the mid-IR spectrum (marked with an asterisk) correspond well to peaks previously assigned to the benzo[ghi]perylene cation in argon by Hudgins & Allamandola (1995a; see also our Table 1). The relative areas of the peaks of neutral before and after photolysis suggests that only ∼15%–20% of the starting benzo[ghi]perylene has been converted to another species, presumably the cation.

The near-IR spectrum of the UV photolyzed H$_2$O-benzo[ghi]perylene mixture presented in Figure 9 contains two strong new absorptions near 13,150 cm^{-1} (0.7605 μm) and 12,100 cm^{-1} (0.826 μm), the latter being twice as broad as the former. The centers of the three near-IR peaks of the benzo[ghi]perylene cation in argon identified by Hudgins & Allamandola (1995a) and Mattioda et al. (2005) at 13,050, 12,480, and 12,190 cm^{-1} (0.766, 0.8013, and 0.8203 μm, respectively) are indicated by dashed vertical lines. The two near-IR peaks we observed for the photolyzed H$_2$O-benzo[ghi]perylene mixture correspond quite well with the shortest and longest wavelength peaks of these electronic transitions of the benzo[ghi]perylene cation in argon. The middle, 12,480 cm^{-1} (0.8013 μm), peak of the benzo[ghi]perylene cation in argon is presumably blended with the longer wavelength peak we observe at 12,190 cm^{-1} (0.8203 μm), and this is why it is broader than the other.

3.1.5. *Naphthalene* (C$_{10}$H$_8$)

The cation of naphthalene was more difficult to detect than those of the previous PAHs studied. We were able to detect only

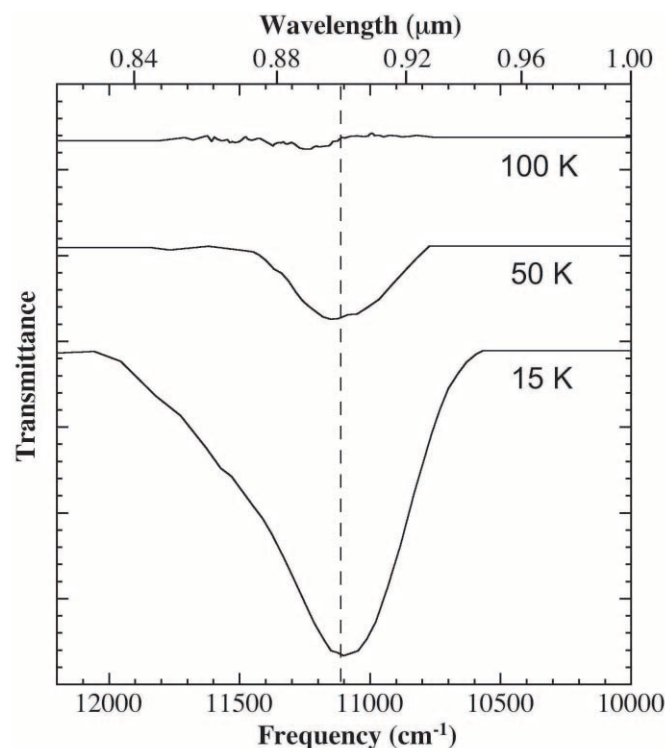the single strongest of the mid-IR absorptions of the naphthalene cation in H$_2$O after photolysis (see below). In addition, we were not able to observe the lowest lying electronic transition of the naphthalene cation in solid H$_2$O, because it falls near 14,500 cm^{-1} (0.690 μm) in H$_2$O ice (Gudipati 2004), slightly longward of its position in an argon matrix (Salama & Allamandola 1991), but still beyond the reach of our near-IR detector.

However, an advantage of naphthalene is that it is volatile enough that one can easily premix it with H$_2$O vapor and control its concentration (§ 2.2). Figure 10 compares the 1230–1200 cm^{-1} (8.13–8.33 μm) portion of the mid-IR spectra of photolyzed H$_2$O-naphthalene mixtures before and after photolysis at two different concentrations (H$_2$O/naphthalene = 10 and 70). In the H$_2$O/naphthalene = 70 case the strength of the putative cation peak at 1217 cm^{-1} (8.217 μm) is greater despite a lower starting neutral naphthalene concentration. Apparently, lower concentrations of naphthalene in H$_2$O permits a higher proportion to be converted to ion, presumably because of fewer naphthalene-naphthalene interactions or less shielding than occurs at higher naphthalene concentrations. The matter is somewhat complicated by the overlap between the cation peak and an absorption of the neutral naphthalene starting material at 1212 cm^{-1} (8.251 μm). As in previous cases, the position of the corresponding band of the cation isolated in argon (Hudgins et al. 1994) is indicated by a dashed vertical line.

4. SUMMARY, DISCUSSION, AND IMPLICATIONS

4.1. *Laboratory Measurements*

Submicron-thick films of five different PAHs (naphthalene, anthracene, phenanthrene, benzo[k]fluoranthene, and
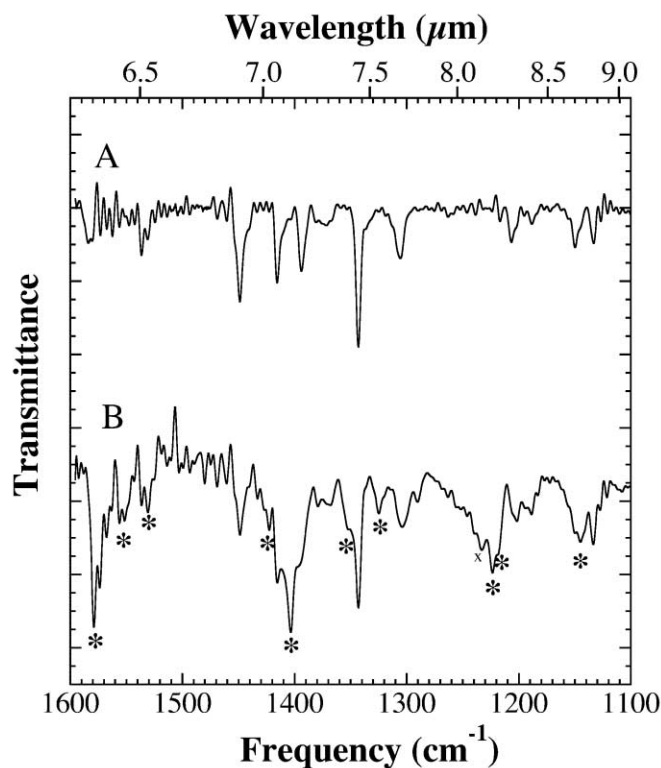
Fig. 8.—The 1600–1100 cm^{-1} (6.25–9.09 μm) IR transmission spectra of the PAH benzo[ghi]perylene (C$_{22}$H$_{12}$) in solid H$_2$O at 15 K (line "A") before and (line "B") after exposure to UV photolysis. The absorptions that increase/appear after photolysis are marked with an asterisk (*) and correspond well to peaks previously assigned to the benzo[ghi]perylene cation in argon by Hudgins & Allamandola (1995a). Thus, we attribute these features to the benzo[ghi]perylene cation in solid H$_2$O. Some of the new absorptions, e.g., near 1400 and 1350 cm^{-1} (7.14 and 7.41 μm) fall on top of preexisting peaks of neutral benzo[ghi]perylene creating uncertainty in the positions, widths, and areas of these peaks (see Table 1). These spectra are displayed on the same scale, but offset for clarity. The peak marked with an "x" is a photoproduct of H$_2$O.

benzo[ghi]perylene) frozen individually at the 1%–3% level in H$_2$O at 15 K and then exposed to UV photolysis show mid-IR absorptions indicative of the formation of PAH cations (see Table 1 for a summary). The positions and relative proportions of these peaks in the mid-IR are consistent with previously measured IR spectra of these cations isolated in argon (Hudgins et al. 1994, 2000; Hudgins & Allamandola 1995a, 1995b) and the greater peak widths are consistent with previously measured mid-IR spectra of PAH neutrals in H$_2$O (Sandford et al. 2004; Bernstein et al. 2005).

In addition, for all but naphthalene, new strong bands were also observed in the near-IR, and these are consistent with previous measurements of electronic transitions of the corresponding PAH cations isolated in argon (Hudgins & Allamandola 1995a, 1995b; Mattioda et al. 2005) and/or in the gas phase (Sukhorukov et al. 2004). Whereas the mid-IR peak positions of the PAH cations in H$_2$O at 15 K were always within the peak width (a few cm^{-1}) of the corresponding absorptions of the PAH cation isolated in argon, the stronger electronic transitions in the near-IR were seen to differ by as much as 180 cm^{-1} (0.02 μm) from those in argon. This behavior is consistent with that observed for other PAHs (Gudipati 2004, and references therein). The greater variance of the position of the near-IR absorptions (compared to the mid-IR) is consistent with the fact that electronic transitions are well-known to be more sensitive to matrix interactions than are vibrational transitions.
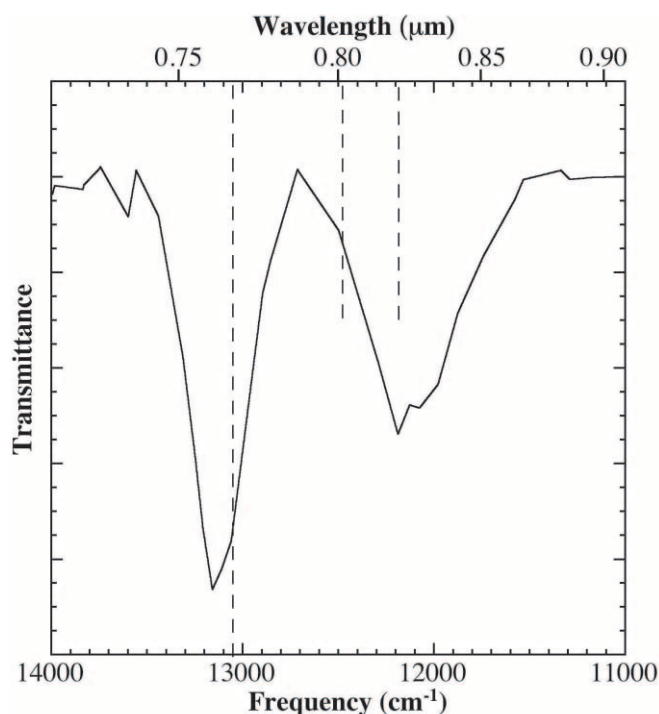

Fig. 9.—The 14,000–11,000 cm^{-1} (0.714–0.909 μm) near-IR transmission spectrum of the PAH benzo[ghi]perylene in solid H$_2$O at 15 K after exposure to UV photolysis. Dashed lines indicate the positions of the absorptions assigned to the benzo[ghi]perylene cation in argon (Hudgins & Allamandola 1995a; Mattioda et al. 2005). The new broad absorption centered near 13,150 cm^{-1} (0.7605 μm) corresponds well to a strong feature at 13,050 cm^{-1} (0.766 μm) assigned to the benzo[ghi]perylene cation in argon. The other new broad band near 12,100 cm^{-1} (0.826 μm) presumably correlates with one or both of two smaller peaks of the cation in argon at 12,480 and 12,190 cm^{-1} (0.8013 and 0.8203 μm).

The peaks attributed to the PAH cations in H$_2$O diminish on warming, but not all at the same temperature; the benzo[k]fluoranthene cation in solid H$_2$O is still present at 100 K, but the phenanthrene cation is not (compare Figs. 5 and 7).

The peak areas of the starting PAHs diminished by up to 40% when exposed to UV photolysis (as seen in Figs. 2, 4, 6, and 8). Presuming that the entire loss of starting material corresponds to formation of the cation, this is a higher ionization efficiency than was observed previously for these same PAHs in argon (Hudgins & Allamandola 1995a, 1995b), but lower than that inferred for other PAHs in H$_2$O by Gudipati & Allamandola (2006). It is reasonable to suppose that there should be a higher proportion ionized in H$_2$O because of its greater capacity to stabilize both the cations and the ejected electrons, and this probably explains why we report higher fractions of the PAHs ionized than did Hudgins & Allamandola (1995a, 1995b) in argon. Furthermore, Figure 10 strongly suggests a concentration effect, with more dilute mixtures of PAHs ionizing to a much greater extent. This may be the explanation for the lower proportion of ions produced in this work where the concentrations were 1%–3%, compared to that reported by Gudipati & Allamandola (2006) where the concentrations were 0.2%–0.5%.

4.2. Astrophysical Implications

IR astronomy suggests aromatics are ubiquitous in the interstellar medium (Allamandola et al. 1999; Cox & Kessler 1999) and the presence of deuterium-enriched and oxidized aromatics in carbonaceous meteorites (Cronin & Chang 1993; Cody & Alexander 2005) and IDPs (Flynn et al. 2004) suggests that
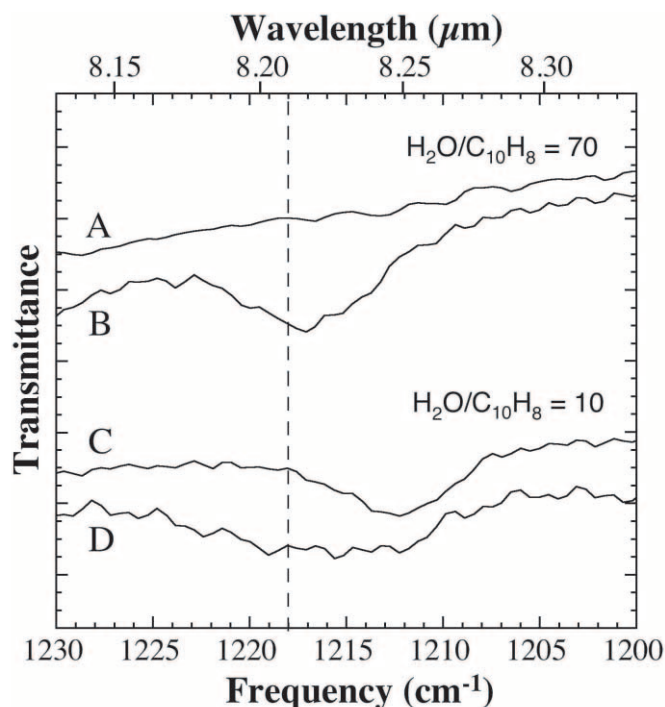
Fig. 10.—The 1230–1200 cm^{-1} (8.13–8.33 μm) IR transmission spectra of an H_2O/naphthalene = 70 ice at 15 K both (line "A") before and (line "B") after exposure to UV photolysis and of an H_2O/naphthalene = 10 ice at 15 K both (line "C") before and (line "D") after exposure to UV photolysis. Neutral naphthalene in H_2O has an absorption at 1212 cm^{-1} (8.251 μm) that is visible in the spectrum of the H_2O/naphthalene = 10 mixture (line C). A new peak centered near 1217 cm^{-1} (8.217 μm) that appears on exposure to UV corresponds very well to that at 1218 cm^{-1} (8.210 μm) assigned to the strongest peak of the naphthalene cation in argon by Hudgins et al. 1994. Note that the efficiency of cation formation is higher in the more dilute ice (see § 4.1 for details).

those aromatics may have experienced radiation at low temperature in H_2O-rich ices (Sandford 2002). The laboratory results reported here confirm that PAHs are ionized by UV in solid H_2O, and show that the resulting PAH cations can be directly observed in the IR. The IR absorptions of neutral aromatics in the ISM have already been observed (Smith et al. 1989; Sellgren et al. 1995; Brooke et al. 1999; Chiar et al. 2000; Bregman et al. 2000).

Given the prevalence of H_2O ice, both in the dense ISM and in the outer solar system, the modest radiation required to produce ions, and their apparent stability at low temperature (at least in pure H_2O), these PAH cations should also be observable in astrophysical ices at near- and mid-IR wavelengths. Interestingly, the strongest mid-IR PAH cation bands fall between 6 and 8 μm, the region in which there are several absorption features in dense clouds that are of uncertain origin (Lacy et al. 1991;

Boogert et al. 1998; Keane et al. 2001). For example, the strong absorptions of the benzo[k]fluoranthene cation could contribute to interstellar absorption seen near 1300 cm^{-1} (7.6 μm) (Boogert et al. 1998). The positions of mid-IR absorptions of PAH cations in H_2O matrices are very similar to those of the corresponding cation in argon, so our mid-IR database of laboratory and modeled spectra (Hudgins et al. 1994, 2000; Hudgins & Allamandola 1995a, 1995b; Langhoff 1996)[2] should provide an adequate guide to PAH cation bands positions and strengths for IR astronomers.

In the near-IR the situation is potentially more problematic; the peak positions of PAH cations in H_2O can shift by as much as 180 cm^{-1} relative to gas-phase/inert matrix positions because of the sensitivity of electronic transitions to matrix interactions. However, the electronic transitions in the near-IR are 10^2–10^3 times stronger than the vibrational absorptions in the mid-IR, so they could be easier to detect telescopically. As noted by Mattioda et al. (2005), these bands could impose detectable weak broadband structure(s) on the interstellar extinction curve, especially near 10,000 cm^{-1} (1 μm). These absorptions are also relevant for H_2O-rich surfaces in the outer solar system where near-IR spectra are most commonly measured and aromatics have been detected, such as in *Cassini* VIMS spectra of Phoebe (Clark et al. 2005) and Iapetus (Cruikshank et al. 2005).

PAH cations in H_2O ices in solar system or protostellar environments where the temperature is above 50 K may not be indefinitely stable. When warmed to 100 K, some cations survive, but some do not (compare Figs. 5 and 7; see also Gudipati & Allamandola 2006). Clearly, temperature stability of a PAH cation will depend on its structure, size, and probably on its concentration in the ice as well.

Combined, these results suggest that it should be possible to use the current database of spectra from Ar matrix-isolated PAH cations to tentatively identify PAHs cations in dense interstellar clouds, around protostars, and on icy satellites in the outer solar system.

---

[2] See also http://www.astrochem.org.

REFERENCES

Allamandola, L. J., Hudgins, D. M., & Sandford, S. A. 1999, ApJ, 511, L115
Allamandola, L. J., & Sandford, S. A. 1988, in Dust in the Universe, ed. M. E. Bailey & D. A. Williams (Cambridge: Cambridge Univ. Press), 229
Bernstein, M. P., Moore, M. H., Elsila, J. E., Sandford, S. A., Allamandola, L. J., & Zare, R. N. 2003, ApJ, 582, L25
Bernstein, M. P., Sandford, S. A., & Allamandola, L. J. 2005, ApJS, 161, 53
Bernstein, M. P., Sandford, S. A., Allamandola, L. J., Gillette, J. S., Clemett, S. J., & Zare, R. N. 1999, Science, 283, 1135
Boogert, A. C. A., Helmich, F. P., van Dishoeck, E. F., Schutte, W. A., Tielens, A. G. G. M., & Whittet, D. C. B. 1998, A&A, 336, 352
Bregman, J. D., Hayward, T. L., & Sloan, G. C. 2000, ApJ, 544, L75
Brooke, T. Y., Sellgren, K., & Geballe, T. R. 1999, ApJ, 517, 883
Chiar, J. E., Tielens, A. G. G. M., Whittet, D. C. B., Schutte, W. A., Boogert, A. C. A., Lutz, D., van Dishoeck, E. F., & Bernstein, M. P. 2000, ApJ, 537, 749

Clark, R. N., et al. 2005, Nature, 435, 66
Cody, G. D., & Alexander, C. M. O. 2005, Geochim. Cosmochim. Acta, 69, 1085
Cox, P., & Kessler, M. F., eds. 1999, The Universe as Seen by *ISO*, Vol. II (ESA SP-427; Noordwijk: ESA)
Cronin, J. R., & Chang, S. 1993, in The Chemistry of Life's Origins, ed. J. Greenberg, C. Mendoza-Gómez, & V. Pirronello (Dordrecht: Kluwer), 209
Cruikshank, D. P., et al. 2005, BAAS, 37, 39.06
———. 2007, Icarus, in press
Flynn, G. J., Keller, L. P., Jacobsen, C., & Wirick, S. 2004, Adv. Space Res., 33, 57
Gudipati, M. S. 2004, J. Phys. Chem. A, 108, 4412
Gudipati, M. S., & Allamandola, L. J. 2006, ApJ, 638, 286
Hudgins, D. M., & Allamandola, L. J. 1995a, J. Phys. Chem. A, 99, 3033
———. 1995b, J. Phys. Chem. A, 99, 8978

Hudgins, D. M., Bauschlicher, C. W., Jr., Allamandola, L. J., & Fetzer, J. C. 2000, J. Phys. Chem. A, 104, 3655
Hudgins, D. M., & Sandford, S. A. 1998a, J. Phys. Chem. A, 102, 329
———. 1998b, J. Phys. Chem. A, 102, 344
———. 1998c, J. Phys. Chem. A, 102, 353
Hudgins, D. M., Sandford, S. A., & Allamandola, L. J. 1994, J. Phys. Chem., 98, 4243
Hudgins, D. M., Sandford, S. A., Allamandola, L. J., & Tielens, A. G. G. M. 1993, ApJS, 86, 713
Jenniskens, P., & Blake, D. F. 1994, Science, 265, 753
Jenniskens, P., Blake, D. F., Wilson, M. A., & Pohorille, A. 1995, ApJ, 455, 389
Keane, J. V., Tielens, A. G. G. M., Boogert, A. C. A., Schutte, W. A., & Whittet, D. C. B. 2001, A&A, 376, 254
Lacy, J. H., Carr, J. S., Evans, N. J., II, Baas, F., Achtermann, J. M., & Arens, J. F. 1991, ApJ, 376, 556
Langhoff, S. R. 1996, J. Phys. Chem., 100, 2819

Mattioda, A. L., Allamandola, L. J., & Hudgins, D. M. 2005, ApJ, 629, 1188
Prasad, S. S., & Tarafdar, S. P. 1983, ApJ, 267, 603
Ricca, A., & Bauschlicher, C. W., Jr. 2000, Chem. Phys. Lett., 328, 396
Salama, F., & Allamandola, L. 1991, J. Chem. Phys., 94, 6964
Sandford, S. A. 2002, Planet. Space Sci., 50, 1145
Sandford, S. A., Bernstein, M. P., & Allamandola, L. J. 2004, ApJ, 607, 346
Sandford, S. A., Bernstein, M. P., Allamandola, L. J., Gillette, J. S., & Zare, R. N. 2000, ApJ, 538, 691
Sellgren, K., Brooke, T. Y., Smith, R. G., & Geballe, T. R. 1995, ApJ, 449, L69
Smith, R. G., Sellgren, K., & Tokunaga, A. T. 1989, ApJ, 344, 413
Sukhorukov, O., Staicu, A., Diegel, E., Rouillé, G., Henning, Th., & Huisken, F. 2004, Chem. Phys. Lett., 386, 259
Szczepanski, J., Vala, M., Talki, D., Parisel, O., & Ellinger, Y. 1993, J. Phys. Chem., 98, 4494
Warneck, P. 1962, Appl. Optics, 1, 721